2003

Millimeter-Wave Spectroscopy of Cold Rb Rydberg Atoms in a Magneto-Optical Trap: Quantum Defects of the *ns*, *np*, and *nd* Series

Wenhui Li

I. Mourachko

Michael Noel
Bryn Mawr College, mnoel@brynmawr.edu

T. F. Gallagher

Custom Citation
W.H. Li, I. Mourachko, M.W. Noel and T.F. Gallagher, *Phys. Rev. A* **67**, 52502 (2003).

Millimeter-wave spectroscopy of cold Rb Rydberg atoms in a magneto-optical trap: Quantum defects of the *ns*, *np*, and *nd* series

Wenhui Li,[1] I. Mourachko,[1] M. W. Noel,[2] and T. F. Gallagher[1]
[1]*Department of Physics, University of Virginia, Charlottesville, Virginia 22904*
[2]*Department of Physics, Bryn Mawr College, Bryn Mawr, Pennsylvania 19010*
(Received 21 June 2002; revised manuscript received 25 November 2002; published 13 May 2003)

By using a magneto-optical trap we have measured the Rb ns-$(n+1)s$ and nd_j-$(n+1)d_j$ two-photon millimeter-wave transitions for $32 \leqslant n \leqslant 37$, observing 100-kHz-wide resonances, in spite of the trap's 10 G/cm magnetic-field gradient, in which one might expect to observe resonances 5 MHz wide. This resolution is possible because of the similarity of the g_j factors in the initial and final states. Under the same conditions, the single-photon *ns*-*np* resonances are ~5 MHz wide. To make useful measurements of these intervals, we turned off the trap field and used the 300-K atoms of the background Rb vapor. Together these measurements improve the accuracy of the *s*, *p*, and *d* quantum defects by an order of magnitude.

DOI: 10.1103/PhysRevA.67.052502 PACS number(s): 32.30.Bv, 32.10.Fn, 32.80.Pj

I. INTRODUCTION

High-resolution spectroscopy of cold trapped Rydberg atoms is interesting, primarily as a probe of interatomic interactions, which are important in several different contexts. For example, a high-resolution probe offers the best hope of detecting fascinating new species, such as the cold Rydberg ''trilobite'' molecules, composed of a cold Rydberg atom and a cold ground-state atom [1,2]. In these molecules, the short-range interaction between the slow Rydberg electron and the ground-state atom provides the potential that binds the two atoms together at large internuclear separations. However, the molecules are not very tightly bound, by at most 100 MHz for a Rb $30d$-Rb $5s$ molecule, so high spectral resolution is essential for their detection. A very different application arises in quantum-information processing. In particular, there have been proposals for quantum-information processing based on the energy shifts from dipole-dipole interactions between Rydberg atoms [3,4]. While dipole-dipole energy shifts have not yet been observed, resonant dipole-dipole energy transfer in frozen Rydberg gases has been [5,6]. In observed energy transfers, though, it was clear that several dipole-dipole interactions were important. More controlled experiments using high-resolution spectroscopic probes would serve to clarify the physics of the observed energy-transfer processes and dipole-dipole interactions in cold Rydberg gases generally. Finally, a series of experiments has shown that ultracold plasmas evolve into cold Rydberg atoms and vice versa, and high-resolution line broadening spectroscopy of Rydberg atoms in these plasmas should be a useful tool in understanding them [7–10]. Although the most interesting aspect of cold Rydberg atoms is the variety of interactions between them, Rydberg series of isolated atoms also offer the possibility of a convenient optical wavelength standard [11]. While the original proposal was based on Doppler-free two-photon spectroscopy of room-temperature atoms, the relative simplicity of producing cold atoms should allow the technique applied to single-photon transitions as well, extending its usefulness into the ultraviolet region. For Rb, the accuracies of the present quantum defects only allow optical accuracy of 50 MHz [12,13]. Better quantum defects are required for improved accuracy.

Here, we report the millimeter (mm)-wave spectroscopy of cold Rb Rydberg atoms in a magneto-optical trap (MOT). Millimeter-wave spectroscopy of Rydberg atoms is not new [14,15], but what is surprising about these measurements is that when observing two-photon transitions we achieve 100-kHz resolution in spite of the trap's magnetic-field inhomogeneity of 10 G/cm, which one would expect to lead to 5-MHz-wide lines. In fact, for single-photon transitions of atoms in the MOT, we do observe 5-MHz-wide lines. The narrow two-photon lines result from the fact that the g_j factors in the initial and final states of a two-photon transition can be the same, so all $\Delta m_j = 0$ transitions occur at the zero-field frequency. The presence of several different m_j states leads unavoidably to different Rabi frequencies, so Rabi oscillations are not visible. Nonetheless, it is still possible to observe Ramsey fringes using separated oscillatory fields and to use them to observe dephasing.

Here we report the use of the two-photon technique to measure the ns-$(n+1)s$ and nd-$(n+1)d$ intervals and derive from them improved quantum defects of the Rb *ns* and *nd* states. Single-photon measurements of *ns*-*np* intervals using room temperature Rb atoms with the MOT fields turned off allows us to determine improved values of the *np* quantum defects as well. In the following sections, we briefly describe our experimental technique, present our experimental results, and describe the procedure used to extract the quantum defects.

II. EXPERIMENTAL APPROACH

The essential idea of the experiment is shown in the level diagram of Fig. 1, in which we use the $35s$-$36s$ transition as an example. ^{85}Rb atoms are held in a vapor loaded MOT, where the trap lasers produce a constant population in the $5p_{3/2}$ state [16]. From the $5p_{3/2}$ state the atoms are excited to the $35s$ Rydberg state with a pulsed dye laser. Immediately after the laser pulse, the atoms are exposed to a mm-wave pulse to drive the $35s$-$36s$ transition, and the presence of $36s$ atoms is detected by selective field ionization.

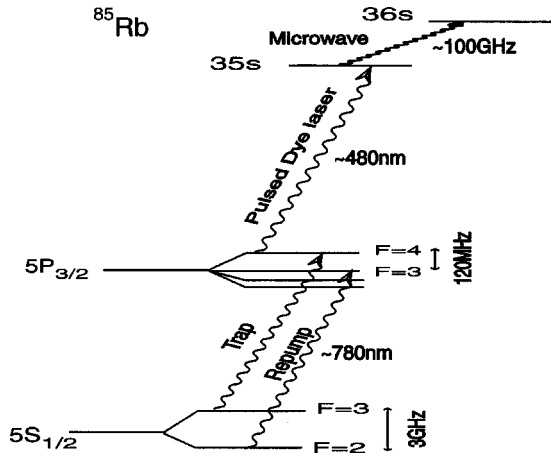

FIG. 1. Energy-level diagram. The $5s_{1/2}$-$5p_{3/2}$ trap transition is excited by a cw diode laser with wavelength 780 nm. Atoms are excited from the $5p_{3/2}$ state to the Rydberg state with a pulsed dye laser of wavelength ~480 nm. A microwave pulse of frequency ~100 GHz is sent into the system immediately after the dye laser.

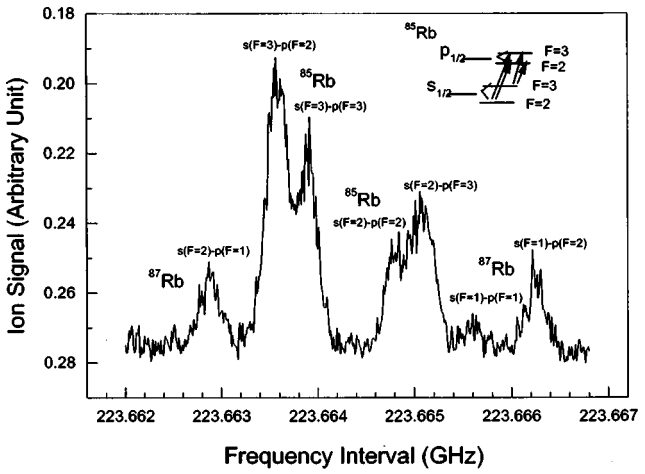

FIG. 2. The observed $27s_{1/2}$-$27p_{1/2}$ spectrum. Instead of using cold atoms in the trap, this spectrum is obtained with the Rb atoms in a 300-K vapor. We use a pulsed 780-nm dye laser to excite the ground-state atoms to the $5p_{3/2}$ state. Since the dye lasers are broadband (~1 cm^{-1}), both ^{85}Rb and ^{87}Rb atoms are excited to Rydberg states, and microwave transitions from both isotopes are visible in this spectrum. The inset shows the allowed transitions for ^{85}Rb.

The MOT is designed for use with microwaves. In particular, the chamber, which is from Kimball Physics, has two 10-cm-diameter windows separated by 12 cm. An electrode structure located midway between the windows consists of four parallel stainless steel rods 0.165 inches in diameter. The rods are vertical, and the centers of the rods pass through the corners of a square 1.78 cm on a side. The atoms trapped in the MOT are in an ellipsoid, of typical dimension ~1 mm, at the center of the four rods. The source of the Rb vapor for the MOT is a set of Rb getters. Both trap and repump lasers are 70-mW Sanyo diode lasers. The trap laser is locked to a ^{85}Rb saturated absorption signal and its output is divided into three beams, each of which has a power of 10 mW before being sent through the chamber and retroreflected back through it. The 480-nm-dye laser is pumped by the third harmonic of an Nd:YAG (yttrium aluminum garnet) laser running at a 20-Hz repetition rate. The dye laser has a linewidth of ~1 cm^{-1}, and a pulse energy of 100 μJ.

To generate the mm waves we generate harmonics of a stable low-frequency source. In particular, we use a Hewlett-Packard 83620A synthesizer to generate frequencies up to 20 GHz. The cw output of the synthesizer is formed into pulses synchronized with the laser using an SRS DG 535 digital delay generator. After amplification to 10 mW peak power by a Miteq MNP4 amplifier, the microwave pulses drive a Narda-DBS-2640×220 active doubler, which produces 100-mW pulses at frequencies between 26 and 40 GHz. The output of the doubler passes through an isolator to a Pacific millimeter W3WO passive tripler, which is optimized for the third harmonic, and generates 1-mW-mm-wave pulses at frequencies up to 120 GHz. At lower, but unspecified power, it generates harmonics up to 225 GHz. The output of the tripler passes through WR10 waveguide to a Hughes precision attenuator and horn, which is used to launch the mm waves through one of the large windows of the vacuum chamber. The mm waves are polarized horizontally to minimize the effect of vertical rods on them.

To observe the 35*s*-36*s* resonance, the dye laser wavelength is set so as to excite the 35*s* state, and we repetitively scan the synthesizer over the 35*s*-36*s* two-photon transition while recording the 36*s* field ionization signal. When the signal-to-noise ratio is adequate we stop the scan and save the data. This procedure is used to observe 100-kHz-wide two-photon ns-$(n+1)s$ and nd-$(n+1)d$ transitions, in spite of the presence of the inhomogeneous trap field, which leads to 5-MHz-wide one-photon *ns*-*np* transitions. To observe narrow resonances for single-photon transitions, we have turned the trap fields off and used the 300-K Rb vapor instead of the trapped Rb atoms. To produce an observable number of Rydberg atoms, we use a pulsed 780 nm dye laser instead of the narrow-band diode laser to excite the ground-state atoms to the $5p_{3/2}$ state.

III. OBSERVATIONS

In Fig. 2 we show a recording of the $27s_{1/2}$-$27p_{1/2}$ transition, obtained with a 300-K vapor of Rb and 8-μs-long microwave pulse, which leads to linewidths of ~0.3 MHz due primarly to Doppler broadening. As shown by Fig. 2, transitions from both hyperfine levels of both ^{85}Rb and ^{87}Rb 27*s* states are visible, as is the hyperfine structure of the $27p_{1/2}$ state. At higher *n*, the hyperfine structure is not completely resolved due to the n^{*-3} scaling of these intervals. Here n^* is the effective quantum number. It is related to the binding energy W and the quantum defect δ by [17]

$$W=\frac{-R_{\mathrm{Rb}}}{n^{*2}}=-\frac{R_{\mathrm{Rb}}}{(n-\delta)^2}, \tag{1}$$

where R_{Rb} is the Rydberg constant for the reduced electron mass in Rb. In Table I we give the frequencies of the centers of gravity of these ns-np_j $(j=1/2,3/2)$ transitions. By center of gravity we mean the frequencies in the absence of hyper-

TABLE I. The frequencies of the centers of gravity of ns-$np_{1/2}$ and ns-$np_{3/2}$ transitions are listed with experimental uncertainties. The last column contains the differences between observed and calculated intervals (residual = observed − calculated).

n	Observed interval (MHz)	Residual (MHz)
	ns-$np(1/2)$ intervals	
27	223 664.264(22)	−0.010
28	197 990.586(25)	0.015
29	176 100.586(20)	0.023
30	157 322.108(22)	−0.009
31	141 121.445(21)	0.005
32	127 070.956(25)	−0.006
33	114 825.466(26)	−0.005
34	104 104.194(27)	0.009
	ns-$np(3/2)$ intervals	
28	203 322.762(40)	−0.033
29	180 848.640(38)	−0.005
30	161 568.406(29)	0.050
31	144 934.120(47)	−0.014
32	130 507.152(34)	−0.025
33	117 933.187(32)	0.003

fine structure (hfs). The ns hyperfine intervals of ^{85}Rb and ^{87}Rb and p fine-structure intervals extracted from the single-photon ns-np data are tabulated in Tables II and III, respectively. The ns hyperfine intervals of ^{85}Rb are represented in this range of n by

$$\nu_{\rm hfs} = 14.6(14)\ \text{GHz}^*(n^*)^{-3}, \tag{2}$$

where n^* is the effective quantum number of the s states. In determining the constant of Eq. (2) we have omitted the 30s hyperfine interval from Table II.

The np fine-structure (fs) intervals of ^{85}Rb are represented by

$$\nu_{\rm fs} = 869\,357(7)\ \text{THz}(n^*)^{-3} - 233(5)\ \text{GHz}(n^*)^{-5}, \tag{3}$$

TABLE II. Rb ns hyperfine intervals.

n	^{85}Rb hfs interval (MHz)	Residual (MHz)
28	0.967(79)	0.018
29	0.841(77)	−0.002
30	0.672(60)	−0.080
31	0.755(92)	0.081
32	0.626(66)	0.019
33	0.547(64)	−0.001
	^{87}Rb hfs interval (MHz)	
28	2.14(10)	
29	1.94(9)	
30	1.56(8)	
31	1.61(13)	
32	1.41(10)	
33	1.26(8)	

TABLE III. p fine-structure intervals.

n	Fine-structure interval (MHz)	Residual (MHz)
28	5332.176(64)	−0.002
29	4748.054(58)	0.005
30	4246.298(51)	0.083
31	3812.676(68)	−0.004
32	3436.196(59)	−0.011
33	3107.721(58)	0.010

where n^* is the effective quantum number of the p states obtained from the center of gravity of the $p_{1/2}$ and $p_{3/2}$ states. In determining the constants of Eq. (3), we have omitted the 30p fine-structure interval from Table III. As shown by Tables II and III these expressions represent the observed intervals within the experimental uncertainties.

The two-photon ns-$(n+1)s$ and nd_j-$(n+1)d_j$ transitions were observed using the MOT, and as an example we show in Fig. 3 the $32d_{5/2}$-$33d_{5/2}$ transition observed with a microwave pulse length of 8 μs. We note that twice the linewidth is 0.12 MHz, the transform limit of the pulse length. The narrow line results from the fact that there is an effective $\Delta m_j = 0$ selection rule (in the nd states the hyperfine structure is negligible). As noted earlier, all the $\Delta m_j = 0$ transitions occur at the same frequency for all magnetic fields due to the g_j factors' being the same in both the $32d_{5/2}$ and $33d_{5/2}$ states ($g_j = 4/5$ for $j = 3/2$ and $g_j = 6/5$ for $j = 5/2$). In contrast, the $\Delta m_j = \pm 1$ and $\Delta m_j = \pm 2$ transitions are spread over a large frequency range, ~5 MHz, by the ~10 G/cm field gradient and are undetectable. The observed nd_j-$(n+1)d_{j'}$, $j' \neq j$ transitions are, of course, almost 10 MHz broad because the g_j factors are different.

The Rb ns Rydberg states differ from the nd states in two ways. First, the hyperfine splitting is not completely negligible and must be taken in account. Second, there is a true $\Delta m_s = 0$ selection rule for the decoupled $ns_{1/2}$-$(n+1)s_{1/2}$ transition, not just an effective selection rule as is the case for the nd states [18]. In earlier mm-wave resonance measurements, Goy *et al.* [19] capitalized on this selection rule

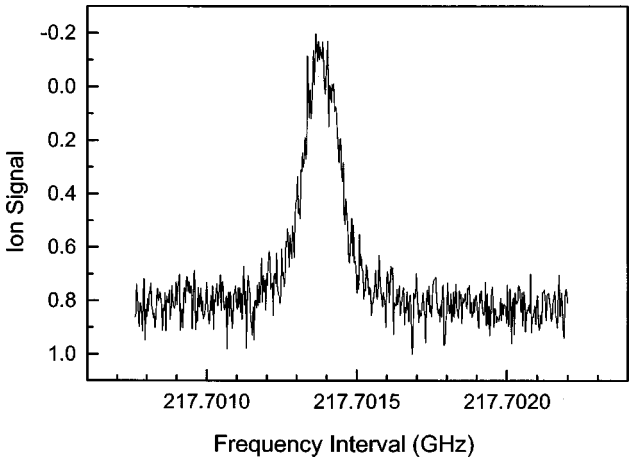

FIG. 3. Two-photon $32d_{5/2}$-$33d_{5/2}$ resonance. The linewidth is 121 kHz, which is about the transform limit of 8-μs-long microwave pulse.

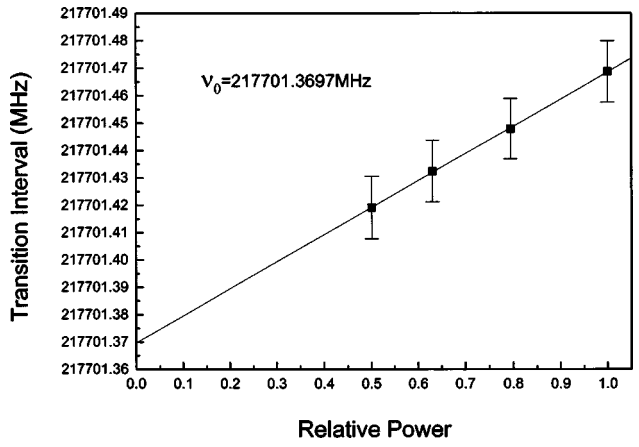

FIG. 4. Extrapolation of the observed $32d_{5/2}$-$33d_{5/2}$ intervals to zero microwave power.

to make high-resolution two-photon mm-wave measurements in the earth's magnetic field.

If there were no hyperfine structure the observed frequencies would be the zero-field intervals. To take into account the hyperfine structure we first note that the $5p_{3/2}$ atoms are predominantly in the $F=4$, $m_f=4$ sublevel, which is driven to the $F=3$, $m_f=3$ sublevel of the *ns* Rydberg state, which has $m_I=5/2$ and $m_s=1/2$. The presence of the zero-field hyperfine splitting shifts this sublevel up in energy by (1/3) $\nu_{\rm hfs} m_s m_i$, which is not a small shift since the hyperfine intervals in this *n* range are of the order 1 MHz. The two-photon microwave transition leaves both m_s and m_I unchanged, so the shift of the observed resonance from the ns-$(n+1)s$ interval in the absence of hyperfine structure is given by

$$\Delta = \tfrac{1}{3}[\,\nu_{\rm hfs}(n) - \nu_{\rm hfs}(n+1)]m_s m_i\,, \tag{4}$$

where $\nu_{\rm hfs}(n)$ is the zero-field hyperfine interval of the *ns* state. Since $\nu_{\rm hfs}(n)$ scales as n^{-3}, the difference between the *ns* and $(n+1)s$ hyperfine intervals is small, and the typical value of Δ is 20 kHz. Using the values of $\nu_{\rm hfs}(n)$ given by Eq. (2), we have corrected the observed intervals before using them to determine the quantum defects.

To extract the intervals from the two-photon transitions we must extrapolate the observed frequencies to zero microwave power. As shown in the example of Fig. 4, the shifts are small, typically tens of kilohertz, but observable. In Tables IV and V, we present the intervals of the ns-$(n+1)s$ and nd_j-$(n+1)d_j$ transitions, extrapolated to zero microwave power.

TABLE IV. ns-$(n+1)s$ two-photon transition intervals. The observed intervals are listed with uncertainties. The corrected intervals are the intervals between the centers of gravity. The last column contains the differences between the observed and calculated values.

n	Observed interval (MHz)	Corrected interval (MHz)	Residual (MHz)
34	213 275.475(20)	213 275.494	−0.002
35	194 106.602(16)	194 106.619	−0.001
36	177 167.944(10)	177 167.959	0.007
37	162 144.314(10)	162 144.327	−0.006

TABLE V. nd_j-$(n+1)d_j$ two-photon transition intervals. The observed frequencies are listed with uncertainties. The last column contains the differences between the observed and calculated values.

n	Observed interval (MHz)	Residual (MHz)
	$nd_{5/2}$-$(n+1)d_{5/2}$ intervals	
30	265 663.444(30)	−0.003
31	240 092.800(10)	−0.001
32	217 701.370(10)	0.002
33	198 010.022(10)	0.009
34	180 623.703(10)	−0.002
35	165 214.782(10)	−0.007
	$nd_{3/2}$-$(n+1)d_{3/2}$ intervals	
32	217 735.221(10)	0.002
33	198 039.854(10)	−0.004
34	180 650.119(10)	0.001
35	165 238.252(10)	0.002

Our primary motivation for embarking on high-resolution mm-wave spectroscopy was to use it as a probe for interactions between the cold atoms, a particular attraction being the possibility of using coherence as a tool. While the fact that all nd_j-$(n+1)d_j$ $\Delta m_j=0$ two-photon transitions occur at the same frequency allows us to make accurate measurements of the frequencies, the transitions for different m_j levels have different Rabi frequencies, and we are not able to observe Rabi oscillations. While multiple Rabi frequencies might seem to preclude using coherence as a tool, using the Ramsey method of separated fields it is still possible to use the coherence [20], and in Fig. 5 we show the $34d_{5/2}$-$35d_{5/2}$ resonance obtained with two 2-μs-long mm-wave pulses separated by 15 μs. The Ramsey pattern is quite apparent,

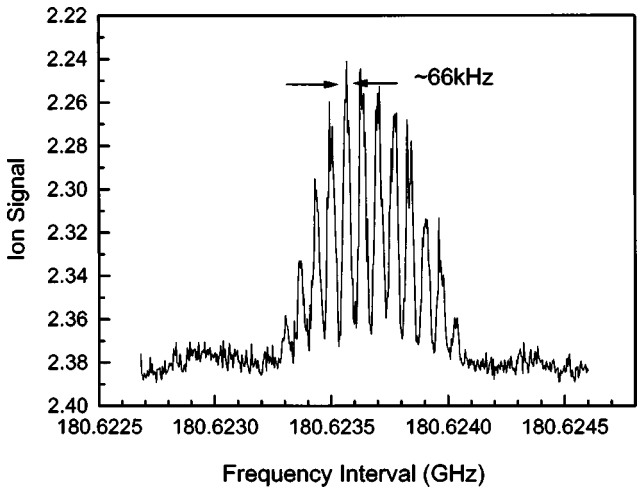

FIG. 5. Ramsey fringes for the $34d_{5/2}$-$35d_{5/2}$ transition observed using two 2-μs-long microwave pulses with a 15-μs delay between them.

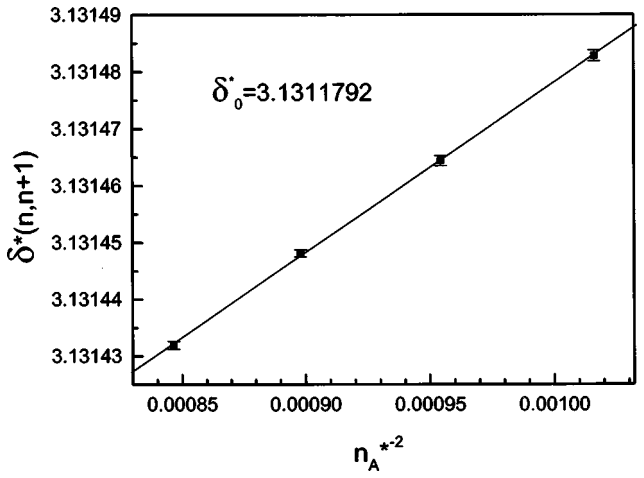

FIG. 6. Plot of the average quantum defect $\delta^*(n,n+1)$ vs n_A^{*-2} for the *ns* states. Here, $n^*=n+0.5-3.131\,09$, and $n=34$–37.

the most important feature being the zeros which occur at the frequencies where the precession of the Bloch vectors during the second mm-wave pulse is exactly opposite to the precession during the first pulse. Even though the precessions of the Bloch vector are different for different m_j, the cancellations of the opposing precessions occur at the same frequencies, leading to 100% fringe contrast. Loss of this contrast is a sensitive probe of dephasing due to interactions with other atoms or charged particles.

IV. EXTRACTION OF THE QUANTUM DEFECTS

The frequency interval $\nu_{nn'}$ between any two states n and n' can be expressed by the Rydberg formula involving the quantum defects of the two levels [17]

$$\nu_{nn'}=R_{\mathrm{Rb}}c\{[n-\delta(n)]^{-2}-[n'-\delta(n')]^{-2}\}, \qquad (5)$$

where $R_{\mathrm{Rb}}=109\,736.605\ \mathrm{cm}^{-1}$, $c=2.997\,924\,58\times10^{10}$ cm/s is the speed of light, and $\delta(n)$ and $\delta(n')$ are the quantum defects of the initial and final states, which mainly depend on ℓ and only slightly on j and n. For given ℓ and j, the quantum defects, for $n>20$, can be represented by [17]

$$\delta(n)=\delta_0+\delta_2/(n-\delta_0)^2, \qquad (6)$$

where δ_0 and δ_2 are constants.

For the two-photon ns-$(n+1)s$ and nd_j-$(n+1)d_j$ transitions, we extract the quantum defects from the observed intervals in several steps. Here, we outline the method using the ns-$(n+1)s$ intervals as an example. We begin in a way similar to the one described by Goy *et al.* [19]. We obtain for each observed interval an "average" quantum defect $\delta^*(n,n+1)$ for the pair of relevant levels by use of the relation,

$$\nu_{n,n+1}=R_{\mathrm{Rb}}c\{[n-\delta^*(n,n+1)]^{-2} -[n+1-\delta^*(n,n+1)]^{-2}\}, \qquad (7)$$

and $\delta^*(n,n+1)$ is plotted in Fig. 6 as a function of n_A^{*-2}, where $n_A^*=n+1/2-3.131\,09$. Here 3.131 09 is the previous value of δ_0 for the ^{85}Rb *ns* series [17]. By extrapolating to $n_A^{*-2}=0$, we obtain a preliminary value of δ_0, $\delta_0^*=3.131\,179\,2$. We insert this value into Eq. (6) for δ_0 to obtain an expression for $\delta(n)$ for each *ns* state. In these expressions, δ_2 is the only variable. Using these expressions for $\delta(n)$ we then solve Eq. (5) for each of the ns-$(n+1)s$ intervals listed in Table IV. We then average the four resulting values of δ_2 to obtain a preliminary value of δ_2, $\delta_2^*=0.1791$. To obtain the final values of δ_0 and δ_2, we systematically varied the values of δ_0 and δ_2 in the vicinity of the preliminary values δ_0^* and δ_2^* to find those which minimize the differences between the observed and calculated two-photon intervals. This approach, often termed the grid search method of nonlinear least-squares fitting, is not elegant, but it is efficient in cases such as ours for which we have reasonably good initial trial values [21]. In Table VI, we give the results of this fit. In the uncertainties of Table VI, we have raised those returned by the fit by 50%. Following the same procedure, we obtain the quantum defects of the $nd_j(j=3/2,5/2)$ states.

TABLE VI. The previous and improved quantum defects for *s*, *p*, and *d* series.

		Previous values	Improved values
$ns_{1/2}$	δ_0	3.131 09(2)[a]	3.131 180 4(10)
		3.131 14(2)[b]	
	δ_2	0.204(8)[a]	0.1784(6)
		0.1891(9)[b]	
$np_{1/2}$	δ_0	2.654 56(15)[a]	2.654 884 9(10)
	δ_2	0.388(60)[a]	0.2900(6)
$np_{3/2}$	δ_0	2.641 45(20)[a]	2.641 673 7(10)
	δ_2	0.33(18)[a]	0.2950(7)
$nd_{3/2}$	δ_0	1.348 135(80)[a]	1.348 091 71(40)
	δ_2	−0.595 53[a]	−0.602 86(26)
$nd_{5/2}$	δ_0	1.346 505(80)[a]	1.346 465 72(30)
	δ_2	−0.595 53[a]	−0.596 00(18)

[a]See Ref. [13] or [17].
[b]See Ref. [12].

Once the quantum defects of the *s* states are known, it is straightforward to extract improved quantum defects of the *p* states from the ns-np_j transition frequencies. For example, to obtain the $np_{3/2}$ quantum defects we insert into Eq. (5) the intervals from Table I and the values for the *ns* quantum defects calculated from Eq. (6), using the *ns* values of δ_0 and δ_2 given in Table VI. This procedure results in the observed quantum defects of for the $np_{3/2}$ series. Plotting them vs $1/n^{*2}$, where $n^*=n-2.641\,45$ (the previous value for δ_0) leads to the graph shown in Fig. 7. In principle, the slope and intercept of Fig. 7 are δ_2 and δ_0 for the $np_{3/2}$ series. This procedure, in which the *ns* quantum defects are treated as known, yields $\delta_0=2.641\,673\,7(3)$ and $\delta_2=0.2950(3)$, which have uncertainties substantially smaller than the uncertainties for δ_0 and δ_2 of the *ns* series. In essence, we have determined the difference of the *ns* and $np_{3/2}$ quantum defects with an uncertainty a factor of 5 smaller than the un-

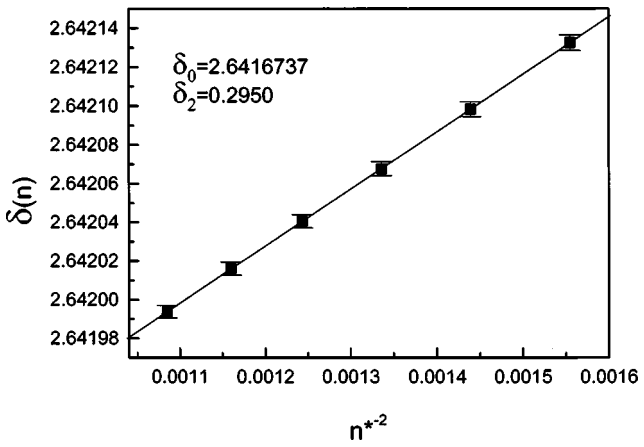

FIG. 7. Plot of $\delta(n)$ vs n^{*-2} for the $np_{3/2}$ states. In this case, $n^*=n-2.641\,45$, $n=28-33$.

certainty in the *ns* quantum defects. The uncertainties of δ_0 and δ_2 for the $np_{3/2}$ series are obtained by adding the uncertainties for the two measurements in quadrature, with the result that the uncertainties of δ_0 for the $np_{3/2}$ states are at most slightly higher than those of the *ns* states.

In Table VI, we list the previous values of the quantum defects and the values we have obtained from our measurements. A consistent set of values for the quantum defects was reported by Lorenzen and Niemax [13] who analyzed their *np* data, the *ns* data of Lee *et al.* [11], and the *nd* data of Stoicheff and Weinberger [12]. Also shown in Table VI are the *ns* quantum defects reported by Stoicheff and Weinberger. The uncertainties given by Lorenzen and Niemax for the *nd* series exceed those originally shown by Stoicheff and Weinberger by a factor of 4, probably because of the difference in the reported ionization limit. To the previously reported *nd* quantum defects, which are for the centers of gravity, we have added the effect of the *nd* fine-structure splitting [17]. Our values are just within the error bars or just outside them for the previous measurements with the exception of that made by Lee *et al.* and reported also by Lorenzen and Niemax. It is instructive to convert the uncertainties in the quantum defects into frequency uncertainties. An uncertainty of 10^{-4} in the quantum defect, a typical value, for the optical measurements, translates into a frequency uncertainty of 40 MHz at $n=34$. The *n* single-photon *np* lines were ~750 MHz wide and the *ns* and *nd* two-photon lines were typically 30 MHz wide, or 60 MHz at twice the frequency. In addition, much of the data was taken at Rb pressures at which the broadening and shift of the lines were up to 30 MHz [12]. The optical measurements are really quite impressive.

Our measurements were carried out at number densities of 10^9 cm^{-3}, roughly five orders of magnitude lower than those used in the optical measurements, and the pressure shifts are not an issue, particularly since the differential shifts between levels are likely to be small. In addition, the frequency control of our source is better, allowing us to improve the accuracy of the quantum defects by an order of magnitude. In the last columns of Tables I–V, we show the differences between the observed transition intervals and the intervals calculated from the improved quantum defects and fine and hyperfine constants. All these differences are within the listed experimental uncertainties.

V. CONCLUSION

These mm-wave measurements of the Δn intervals between Rb Rydberg states lead to improvements of an order of magnitude in the quantum defects. Probably more important, they show that it is possible to do high-resolution spectroscopy in spite of the large magnetic-field gradient in the MOT. The fact that such high resolution is possible suggests that mm-wave resonance spectroscopy should be a sensitive probe for investigating many-body effects in cold Rydberg atom samples.

ACKNOWLEDGMENTS

This work has been supported by the Air Force Office of Scientific Research. It is a pleasure to acknowledge helpful discussions with R. R. Jones, C. A. Sackett, and W. E. Cooke.

[1] C. H. Greene, A. S. Dickinson, and H. R. Sadeghpour, Phys. Rev. Lett. **85**, 2458 (2000).
[2] B. E. Granger, E. H. Hamilton, and C. H. Greene, Phys. Rev. A **64**, 042508 (2001).
[3] D. Jaksch, J. J. Girac, P. Zoller, S. L. Rolston, R. Côté, and M. D. Lukin, Phys. Rev. Lett. **85**, 2208 (2000).
[4] M. D. Lukin, M. Fleishauner, R. Côté, L. M. Duan, D. Jaksch, J. J. Cirac, and P. Zoller, Phys. Rev. Lett. **87**, 037901 (2001).
[5] W. R. Anderson, J. R. Veale, and T. F. Gallagher, Phys. Rev. Lett. **80**, 249 (1998).
[6] I. Mourachko, D. Comparat, F. de Tomasi, A. Fioretti, P. Nosbaum, V. Akulin, and P. Pillet, Phys. Rev. Lett. **80**, 253 (1998).
[7] T. C. Killian, M. J. Lim, S. Kulin, R. Dumke, S. D. Bergeson, and S. L. Rolston, Phys. Rev. Lett. **86**, 3759 (2001).
[8] M. P. Robinson, B. Laburthe Tolra, M. W. Noel, T. F. Gallagher, and P. Pillet, Phys. Rev. Lett. **85**, 4466 (2000).
[9] S. Mazevet, L. A. Collins, and J. D. Kress, Phys. Rev. Lett. **88**, 055001 (2002).
[10] F. Robischeaux and J. D. Hansen, Phys. Rev. Lett. **88**, 055002 (2002).
[11] S. A. Lee, J. Helmcke, J. L. Hall, and B. P. Stoicheff, Opt. Lett. **3**, 141 (1978).
[12] B. P. Stoicheff and E. Weinberger, Can. J. Phys. **57**, 2143 (1979).
[13] C. J. Lorenzen and K. Niemax, Phys. Scr. **27**, 300 (1983).
[14] P. Goy, J. M. Raimond, G. Vitrant, and S. Haroche, Phys. Rev. A **26**, 2733 (1982).
[15] F. Merkt and H. Schmutz, J. Chem. Phys. **108**, 10 033 (1998).
[16] C. Monroe, W. Swann, H. Robinson, and C. Wieman, Phys. Rev. Lett. **65**, 1571 (1990).

[17] T. F. Gallagher, *Rydberg Atoms* (Cambridge University Press, Cambridge, 1994).
[18] N. Bloembergen and M. D. Levenson, in *High Resolution Laser Spectroscopy*, edited by K. Shimoda (Springer-Verlag, Berlin, 1976), p. 315.
[19] P. Goy, C. Fabre, M. Gross, and S. Haroche, J. Phys. B **13**, L83 (1980).
[20] N. F. Ramsey, *Molecular Beams* (Oxford University Press, Oxford, 1956).
[21] P. R. Bevington and D. K. Robinson, *Data Reduction and Error Analysis for the Physical Sciences* (McGraw-Hill, New York, 1992), pp. 144–147.